Robotica (2008) volume 26, pp. 177–188. © 2007 Cambridge University Press
doi:10.1017/S0263574707003736 Printed in the United Kingdom

LMS robotic hand grasp and manipulation planning (an isomorphic exoskeleton approach)

D. Chaigneau, M. Arsicault*, J.-P. Gazeau and S. Zeghloul

Laboratoire de Mécanique des Solides (LMS), UMR CNRS 6610, Université de Poitiers, SP2MI, 2 Bd Pierre et Marie Curie, BP 30179, 86962 Futuroscope Chasseneuil Cedex, France

(Received in Final Form: April 17, 2007. First published online: August 21, 2007)

SUMMARY

In order to widen the potentialities of manipulation of the Laboratoire de Mécanique des solides (LMS) mechanical hand, we developed a new planning approach based on the use of a specific exoskeleton. This one has kinematics architecture and dimensions identical to the mechanical hand. This feature allows us to obtain manipulation trajectories for the mechanical hand, very easily and very quickly, by using the exoskeleton, without complex calibration. Manipulation's trajectories are replayed offline with an autonomous control, and, consequently, the exoskeleton is not used with any feedback strategy for telemanipulation. This paper presents the characteristics of this exoskeleton and the graphic interface that we developed. This one uses a method to determine the object's evolution during the manipulation with the exoskeleton, without using exteroceptive sensors. This new approach was tested for standard trajectories by simulation on a Computer-aided design (CAD) robotics system and by using the mechanical hand. Thus, we validate the use concept of an isomorphic exoskeleton to mechanical hand for manipulation planning with the LMS mechanical hand.

KEYWORDS: Dexterous hand; Exoskeleton hand; Manipulation task.

1. Introduction

The current study will allow us to plan the manipulation task for Laboratoire de Mécanique des solides (LMS) mechanical hand using an innovative learning technique based on the use of a specific exoskeleton. The existing literature deals with the various learning methods and devices that allow the complete or the partial description of the human fingers' motion during the manipulation task. To recover the whole postures of the human hand during the execution of a manipulation task, the exoskeletons[1–6] or the data gloves[7–9] are usually used. These devices are used with various aims such as the immersion in virtual worlds, the teleoperation, or more specifically for rehabilitation and sign language translation. They use various feedback strategies such as force or tactile feedback for most trends, and, more recently, visual or auditive feedbacks. It is obvious, as described in refs. [10–13] that the data gloves and the exoskeletons require a calibration phase and a good model of the human hand to accurately know the position of the operator's fingers. Moreover, in the mechanical hands research area, an additional stage is necessary to map the joint parameters of the operator's fingers to mechanical hand's joint parameters.[2–12] This mapping strongly degrades the potentialities of the slave system and leads to many errors related to the scale factor. In addition, the difference in the kinematics architecture also leads to errors. The use of an isomorphic exoskeleton to the mechanical hand, with unit homothetic ratio, allows us to avoid these problems. Therefore, our goal is to use the skill (the address, the ingenuity, and the intelligence) of a human operator to take advantage of the dexterity of the mechanical hand. Thus, the operator manipulates the objects with a potential dexterity, which is very close to that of the mechanical hand, using his experience, skill, and adaptation capacities to achieve a task with the exoskeleton. The movements transmitted by the operator to the exoskeleton will, however, be limited by the exoskeleton's kinematics. However, the operator's capacity to adapt to this device will enable him to exploit the potentialities of the exoskeleton and, consequently, those with the mechanical hand. On the basis of this observation, we only use this exoskeleton to quickly constitute a database of various trajectories. In a preoccupation of analysis and a planning of these trajectories for a later execution on the mechanical hand, we developed a method to determine the object's evolution during the manipulation with the exoskeleton, without using exteroceptive sensors.

In Section 2, this paper summarily presents the mechanical hand of the LMS and, in particular, the exoskeleton that we manufactured recently. Section 3 presents the model used for the three-dimensional (3D) simulation of various grasped objects as well as for the object manipulation planning with the mechanical hand. In Section 4, we give some examples of trajectories executed by the exoskeleton and reproduced by the mechanical hand. Finally, we discuss the results to show the interest of such an approach.

2. LMS Mechanical Hand and ITs Exoskeleton

In 1996, LMS developed an articulated mechanical hand with four fingers and 16 degrees of freedom (dof). While designing this hand, we tried to reproduce part of the

* Corresponding author. E-mail: Marc.Arsicault@lms.univ-poitiers.fr

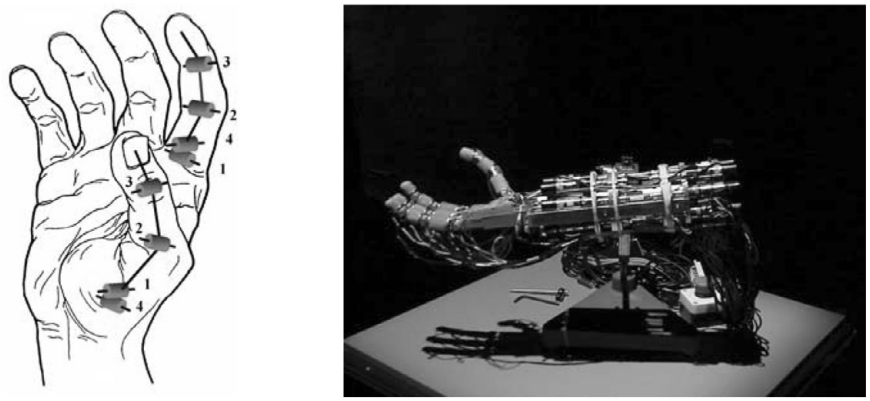

(a) (b)

Fig. 1. (a) Simplified kinematics of human hand. (b) Mechanical Hand of LMS.

anthropomorphic character of the human hand by copying, as well as possible, the flexion-extension and abduction-adduction motions (Fig. 1a). In addition, the layout of the fingers on the palm and the phalanxes' dimensions are similar to those of an average-size human hand. Therefore, the developed mechanical hand (Fig. 1b) generates the standard postures of the human hand as shown in Fig. 2. This behavior is obtained by using the CAD robotics system [System of Modeling and Animation of Robots (SMAR)] developed by the LMS.[14] The mechanical hand has a reliable position and affords low-level control of the fingers.[15] A high-level control deals with the manipulation task planning. It lays down the control rules of the various fingers (kind of control and coordination). A module dedicated to the planning of a manipulation task was also developed within the SMAR software.[16] This module uses a strategy of manipulation based on the geometry and the type of the contact between the object and the fingertips. The first results showed the performance of the proposed method for simple manipulation tasks (translations or rotations of objects) using three fingers only.

The resolution of the grasp stability problem has been developed recently in order to calculate the grasping forces in real time during the execution of the manipulation task.[17] A synthesis method based on the genetic algorithms is developed currently to solve the problem of the initial grasp

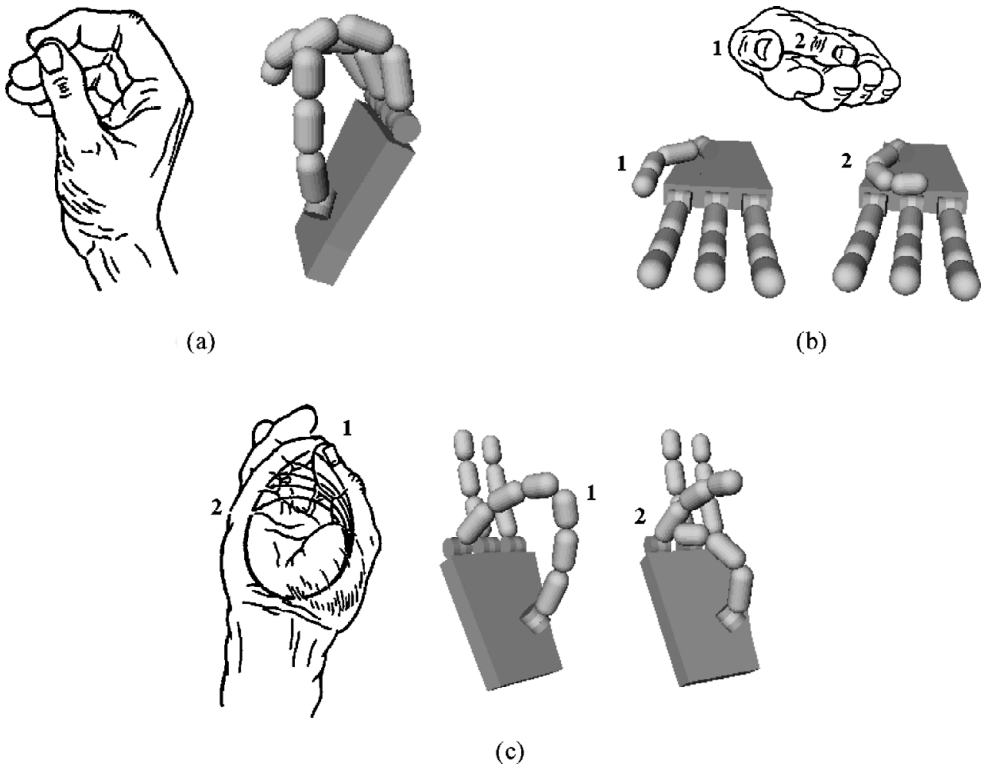

(a) (b) (c)

Fig. 2. SMAR simulation of various configurations of the hand. (a) Pinch. (b) Small stroke of the thumb. (c) Stroke of a maximum opposition of the thumb.

https://doi.org/10.1017/S0263574707003736 Published online by Cambridge University Press

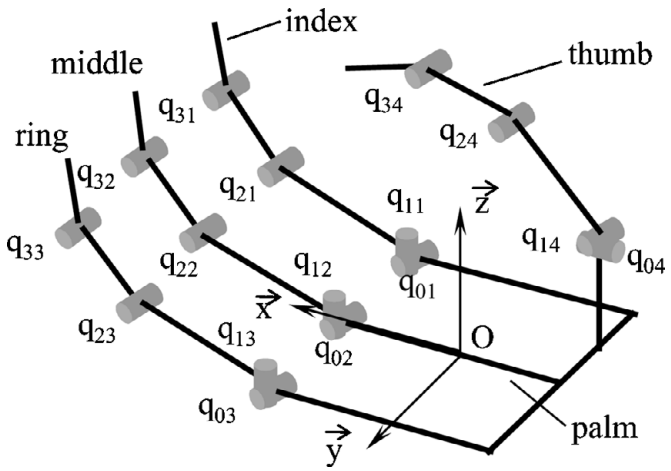

Fig. 3. Kinematics of the exoskeleton.

and the regrasping using the fourth finger. Thus, these whole developments enable us to establish the complete planning of the manipulation task with the mechanical hand. We present in this paper another approach that uses a specific exoskeleton to obtain the manipulation trajectories. Figure 3 shows the kinematics of this exoskeleton. This kinematics and the dimensions of the phalanxes are identical to those of the LMS mechanical hand, i.e., the exoskeleton is isomorphic to the LMS mechanical hand with unit homothetic ratio. The annotations specified in Fig. 3 are those used in the rest of the paper. This exoskeleton is composed of four kinematic chains with four degrees of freedom for each one of three fingers and the thumb. The amplitudes of the flexion-extension movement and abduction-adduction movement are identical to those of the mechanical hand, and the lengths of the phalanxes are also respected. The abduction-adduction movement is placed after the flexion-extension movement for the fingers while those movements are inverted for the thumb.

As shown in Fig. 4, the distal phalanxes of the operator's hand are placed in gussets that have the size and the external shape identical to the distal phalanxes of the mechanical hand. The properties of contacts obtained with the exoskeleton are similar to those of the mechanical hand. The wrist of the operator is strapped; the rest of the hand is free. The developed exoskeleton is passive and, during manipulation, only the joint position parameters are recorded using 16 potentiometers. These sensors are located away from the articulations so as not to block the motion of the fingers.

The acquisition frequency of the articular parameters is 50 Hz. An interface board between the personal computer and the exoskeleton allows us to adjust gain and the offset to adapt the sensor's signal. The data are recorded during the task, i.e., the initial grasp, the manipulation, and the repositioning of the fingers on the object. They constitute a knowledge base that is analyzed and exploited thereafter. For the study presented here, the exoskeleton joint values are stored in a database to be analyzed on the one hand, and exploited graphically, in real time, by CAD software (SMAR system) on the other. Figure 5 shows the complete system that allows trajectory planning of the mechanical hand by using the exoskeleton. The grasp stability calculation is not dealt with here. In ref. [17], we deal with the object stability during the object trajectory planning using the CAD tool. For this, we check that the successive grasps, generated during the object manipulation, are of force-closure type. For contacts with friction, the choice of an initial grasp with one finger in opposition to the others is sufficient to check this constraint in most manipulations. This method is also implemented for trajectory planning using the exoskeleton. The mechanical hand, thus, reproduced several trajectories of various manipulated objects obtained with the exoskeleton. The behavior of the mechanical hand, using the exoskeleton trajectories, was satisfactory. This method is easy to implement and it is extremely rapid to obtain manipulation tasks without having to define the object's trajectories.

3. 3D Simulation

The first stage consists in modeling the exoskeleton as accurately as possible. For this, we used a specific module dedicated to the articulated hands, which is available on the SMAR software. Then, we developed a new application which allows the acquisition and the exploitation of the articular parameters of the exoskeleton. After identifying the handled object and the initial grasp, the evolution of the points of contact during manipulation, and, consequently, the calculation of the six operational coordinates of the object can be determined using the articular parameters of the exoskeleton. Figure 6 shows the following stage that

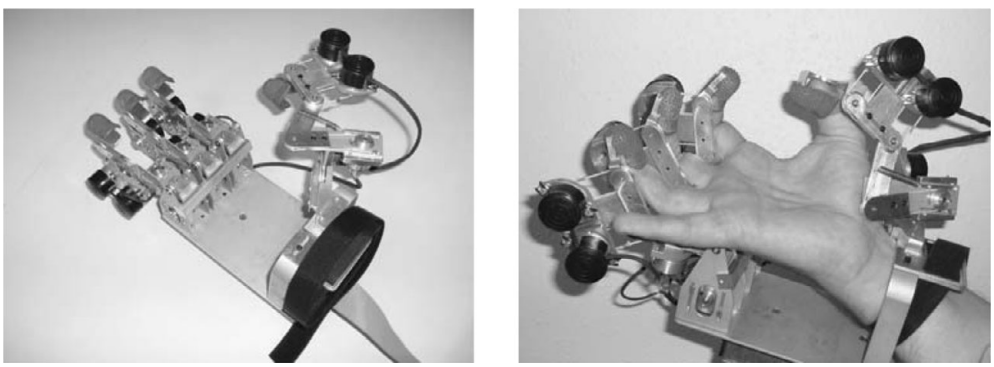

Fig. 4. Exoskeleton of the LMS.

https://doi.org/10.1017/S0263574707003736 Published online by Cambridge University Press

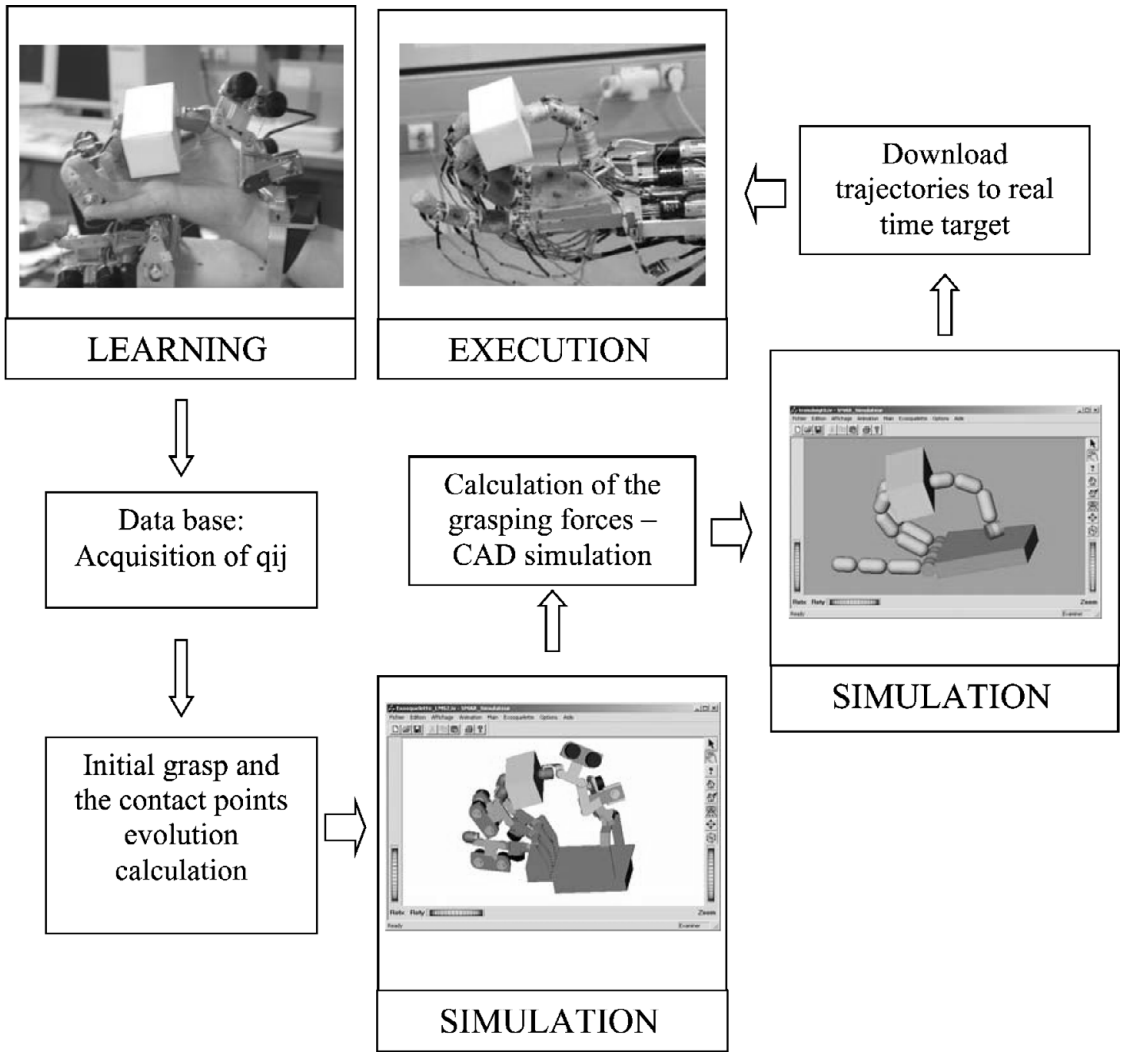

Fig. 5. Diagram of the complete system: exoskeleton/CAD/mechanical hand.

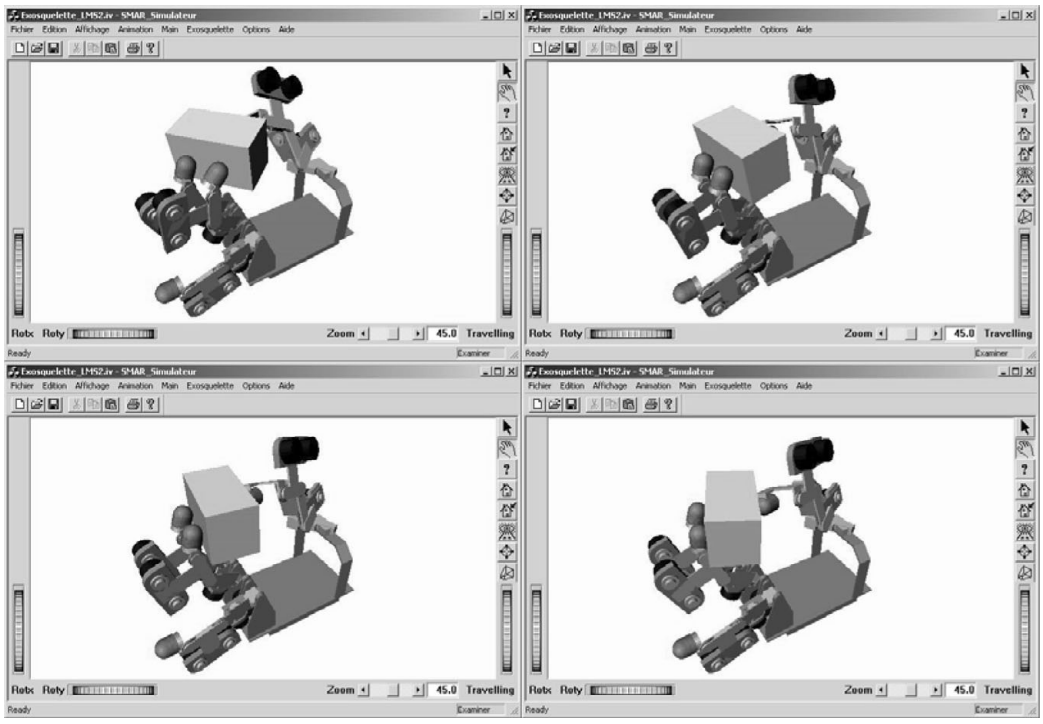

Fig. 6. Rotation of a parallelepiped object produced by the exoskeleton.

https://doi.org/10.1017/S0263574707003736 Published online by Cambridge University Press

concerns the graphic simulation of the exoskeleton and the object.

In this approach, the object's trajectory is obtained only by the parameters of the exoskeleton, contrary to a direct planning by the CAD tool where the trajectory of the object is known beforehand. In Section 3.1, for an object whose geometry and dimensions are known, we show how the evolution of the points of contacts is obtained during the manipulation task, starting from an initial grasp. Section 3.2 indicates how the objects handled are parameterized in order to determine the positions of the contact points for the initial grasps.

3.1. Evolution of the contact points during manipulation

The movement of the object resulting from the fingers' motion has to be known to analyze it on the one hand, and to create its graphic simulation on the other. In order to know the movement of the object resulting from the fingers' motion, we have adapted the method proposed by J. Kerr and B. Roth[18] briefly described later. In this approach, the motion of each finger is determined in order to obtain the desired object motion. Each finger is regarded as an independent manipulator, which has to follow the movement of the object. The shape of the fingertip and the shape of the object are supposed to be unspecified. The contacts are assumed with friction. With the assumption of pure rolling (without sliding) between the object and the fingertip, the paths of the contact points on each surface will be determined by: the geometry of each surface, the motion of the object, and the kinematics of the finger. Because of the nonholonomic constraint of rolling, the equations relating the motion of the object to the motion of the fingertip are expressed by the velocity model of the two bodies. By using the parameters of Fig. 7, we, thus, obtain the following equations:

$$ {}^{P}O_{\mathrm{T}} + {}^{\mathrm{T}}C = {}^{P}O_{\mathrm{B}} + {}^{B}C \tag{1} $$

$$ {}^{\mathrm{T}}\mathbf{n} = {}^{B}\mathbf{n} \tag{2} $$

$$ \mathbf{V}_{\mathrm{T}}(\mathrm{q}) + \boldsymbol{\omega}_{\mathrm{T}} \wedge {}^{\mathrm{T}}\mathrm{C} = \mathbf{V}_{\mathrm{B}}(\mathrm{X}) + \boldsymbol{\Omega}_{\mathrm{B}} \wedge {}^{B}\mathbf{C}. \tag{3} $$

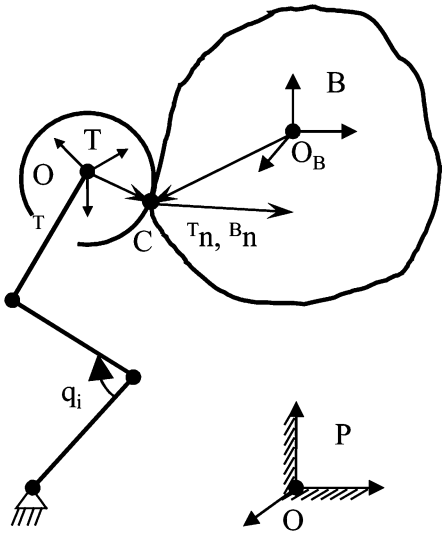

Fig. 7. A finger constrained to roll on the object.

Relation (1) represents the coordinates of the contact point **C** in the frame **P** while passing by the finger (frame **T** whose origin is O_{T}, which is attached to the fingertip) or by the object (frame **B** whose origin is O_{B}, which is attached to the body). The equality of normals ${}^{\mathrm{T}}\mathbf{n}$ and ${}^{B}\mathbf{n}$ at the contact point **C** is expressed by the Eq. (2). The surface at the contact point C on the finger and on the object is described respectively, by the variables $(\boldsymbol{\alpha}, \boldsymbol{\beta})$ and $(\boldsymbol{\eta}, \boldsymbol{\zeta})$. Relation (3) gives the equality of the velocities at the contact point **C**, resulting from rolling constraint.

For this application, we consider that only three fingers are involved in the grasp and that the contact with the object is obtained by the hemispherical shape of the fingertips. The preceding system has 24 equations and only 18 unknowns. These unknowns are the six operational coordinates of the object, for each contact point the variables $(\boldsymbol{\alpha}, \boldsymbol{\beta})$ and the variables $(\boldsymbol{\eta}, \boldsymbol{\zeta})$. For each finger in contact with the object, we finally obtain the following system of eight equations since the normal vectors are defined by two independent components (2′) (see the Appendix for details)

$$ {}^{P}O_{\mathrm{T}} + {}^{P}A_{\mathrm{T}} \cdot {}^{\mathrm{T}}C = {}^{P}O_{B} + {}^{P}A_{B} . {}^{B}C \tag{1′} $$

$$ {}^{P}A_{\mathrm{T}} \cdot {}^{\mathrm{T}}n = {}^{P}A_{\mathrm{B}} \cdot {}^{B}n \tag{2′} $$

$$ \delta O_{\mathrm{T}} + \left({}^{P}J_{\omega}(q^{i-1}) \cdot \delta q^{i}\right) \wedge \left({}^{P}A_{\mathrm{T}}^{i-1} \cdot {}^{\mathrm{T}}C^{i-1}\right) = \delta O_{B} + \left({}^{P}A_{B}^{i-1} \cdot \delta\theta\right) \wedge \left({}^{P}A_{B}^{i-1} \cdot {}^{B}C^{i-1}\right). \tag{3′} $$

To solve this system, it is necessary to introduce six new unknowns in order to obtain a nonlinear system of 24 equations with 24 unknowns. An intuitive solution is to consider six joint parameter unknowns among the 12 given by the exoskeleton, which offers a large possibility of choices that are discussed in Section 4. The obtained nonlinear system (24 equations and 24 unknowns) is then solved by the Newton–Raphson method. Finally, we determine angles defining the orientation of the object **B** with respect to the frame **P** at each motion step. For each motion step, the orientation change can be defined by the orientation vector $\delta\theta$. As $\delta\theta$ is small, the orientation corresponding matrix can, thus, be written

$$ A_{\theta} = \begin{bmatrix} 1 & -\delta\theta_z & \delta\theta_y \\ \delta\theta_z & 1 & -\delta\theta_x \\ -\delta\theta_y & \delta\theta_x & 1 \end{bmatrix}. $$

Hence

$$ {}^{P}A_{B} = {}^{P}A_{B}^{i-1} \cdot A_{\theta} = \begin{bmatrix} A_{11} & A_{12} & A_{13} \\ A_{21} & A_{22} & A_{23} \\ A_{31} & A_{32} & A_{33} \end{bmatrix} $$

where ${}^{P}A_{B}^{i-1}$ is the orientation matrix of the object at the previous step (iteration $i-1$).

We use the following notations: $C\varphi_i$ and $S\varphi_i$ denote $\cos\varphi_i$ and $\sin\varphi_i$, respectively.

https://doi.org/10.1017/S0263574707003736 Published online by Cambridge University Press

The object's orientation angles are obtained by identification of the matrix ${}^{P}A_{B}$ with pitch, yaw, and roll matrix

$$\varphi_1 = \text{ATAN 2}\left(\left(\frac{-A_{23}}{C\varphi_2}\right), \left(\frac{A_{33}}{C\varphi_2}\right)\right)$$
$$\varphi_2 = \text{ASIN}\,(A_{13})$$
$$\varphi_3 = \text{ATAN 2}\left(\left(\frac{-A_{12}}{C\varphi_2}\right), \left(\frac{A_{11}}{C\varphi_2}\right)\right)$$

The iterative method that we present requires the knowledge of the previous configuration. It is, thus, necessary to initialize the algorithm to obtain the trajectory of the object. In particular, it is necessary to know the initial configuration of the object, i.e., the initial grasp.

3.2. The initial grasp

To start the iterative process we need the initial grasp i.e., the initial position and orientation of the object with respect to the frame **P** linked to the exoskeleton palm. This problem is solved by using Eqs. (1) and (2) from the preceding system. Indeed, the condition of rolling without sliding is no longer of any interest since, the initial grasp is static. For this system of 15 independent equations, the number of unknowns that have to be determined is unchanged, and is equal to 18. In the following paragraphs, we show that the knowledge of the geometry of the object associated to the partial knowledge of the position of the initial contact points on the object make it possible to completely determine the initial grasp. In order to obtain the initial grasp parameters without the use of any other external sensors, we considered objects whose shape is *a priori* known, i.e., parallelopiped, cylinder, or sphere.

3.2.1. Parallelopiped. For a parallelopiped, we consider that two fingers are in contact with the same side of the parallelopiped while the thumb is in contact with the opposite side.

In Cartesian coordinates, the partial knowledge of the contact's point in frame **B** is defined in Fig. 8. Then, the position of contact points $\mathbf{C}_i$ is written

$${}^{B}C_1 = \begin{bmatrix} L/2 - e \\ \ell/2 \\ a - H/2 \end{bmatrix}, \quad {}^{B}C_2 = \begin{bmatrix} x_2 \\ -\ell/2 \\ b - H/2 \end{bmatrix}, \text{ and}$$
$${}^{B}C_3 = \begin{bmatrix} x_3 \\ -\ell/2 \\ c - H/2 \end{bmatrix}$$

where ℓ, x_2, and x_3 are the three unknowns.

By considering these new parameters into Eqs. (1′) and (2′), we obtain a system of 15 independent equations with 15 unknowns.

The normal vectors at the contact points are then expressed by

$${}^{B}n_1 = \begin{bmatrix} 0 \\ 1 \\ 0 \end{bmatrix}, {}^{B}n_2 = \begin{bmatrix} 0 \\ -1 \\ 0 \end{bmatrix}, {}^{B}n_3 = \begin{bmatrix} 0 \\ -1 \\ 0 \end{bmatrix}.$$

3.2.2. Cylinder. For a cylinder, the partial knowledge of the contact's point in frame **B** is defined in Fig. 9. Then, the position of contact points $\mathbf{C}_i$ is written

$${}^{B}C_1 = \begin{bmatrix} R \\ 0 \\ a \end{bmatrix}, \quad {}^{B}C_2 = \begin{bmatrix} R\ C\psi_2 \\ R\ S\psi_2 \\ b \end{bmatrix}, \quad {}^{B}C_3 = \begin{bmatrix} R\ C\psi_3 \\ R\ S\psi_3 \\ c \end{bmatrix}$$

where R, ψ_2, and ψ_3 are the three unknowns.

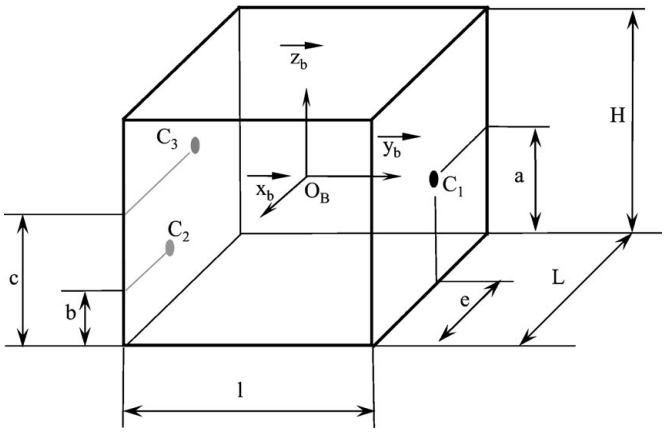

Fig. 8. Modeling of the grasp of parallelopiped.

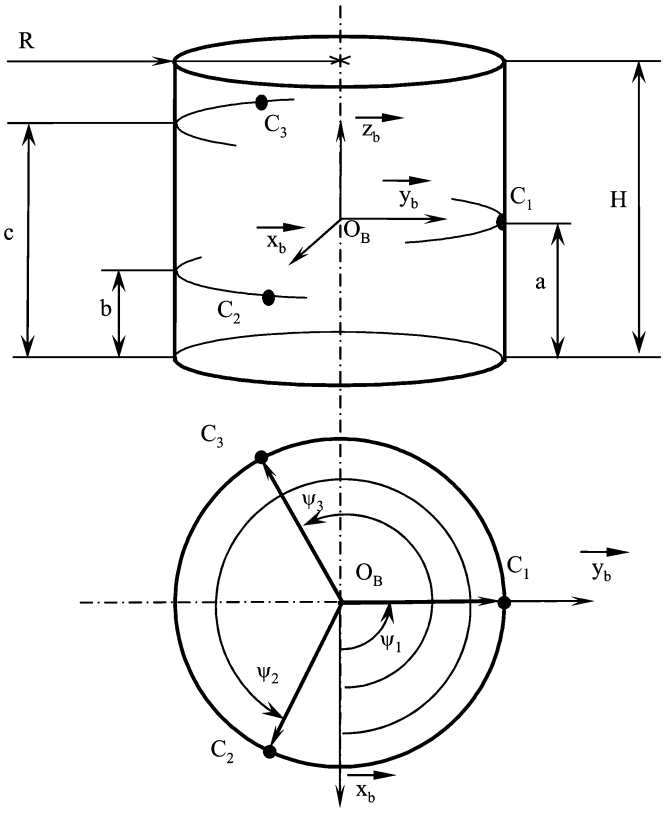

Fig. 9. Modeling of the grasp of a cylinder.

https://doi.org/10.1017/S0263574707003736 Published online by Cambridge University Press

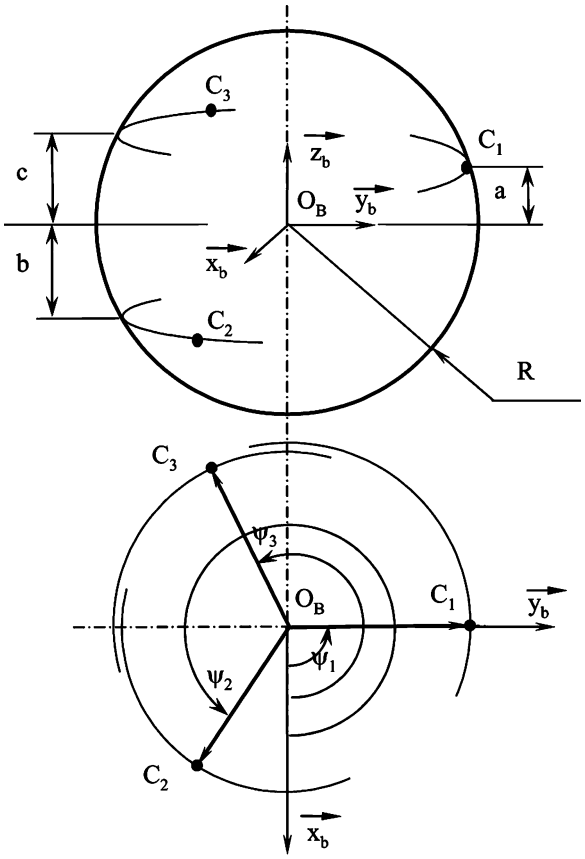

Fig. 10. Modeling of the grasp of a sphere.

By considering these new parameters into Eqs. (1′) and (2′), we obtain a system of 15 independent equations with 15 unknowns.

The normals at the contact points are expressed then by

$$ {}^{B}n_1 = \begin{bmatrix} C\psi_1 \\ S\psi_1 \\ 0 \end{bmatrix}, \quad {}^{B}n_2 = \begin{bmatrix} C\psi_2 \\ S\psi_2 \\ 0 \end{bmatrix}, \quad {}^{B}n_3 = \begin{bmatrix} C\psi_3 \\ S\psi_3 \\ 0 \end{bmatrix}. $$

3.2.3. Sphere. For a cylinder, the partial knowledge of the contact's point in frame **B** is defined in Fig. 10. Then, the position of contact points $\mathbf{C}_i$ is written

$$ {}^{B}C_1 = \begin{bmatrix} \sqrt{R^2 - a^2} \\ 0 \\ a \end{bmatrix}, \quad {}^{B}C_2 = \begin{bmatrix} (\sqrt{R^2 - b^2})\, C\psi_2 \\ (\sqrt{R^2 - b^2})\, S\psi_2 \\ b \end{bmatrix}, $$

$$ {}^{B}C_3 = \begin{bmatrix} (\sqrt{R^2 - c^2})\, C\psi_3 \\ (\sqrt{R^2 - c^2})\, S\psi_3 \\ c \end{bmatrix} $$

where R, ψ_2, are ψ_3 are the three unknowns.

By considering these new parameters into Eqs. (1′) and (2′), we obtain a system of 15 independent equations with 15 unknowns.

The normals at the contact points are expressed then by

$$ {}^{B}n_1 = 1/R \begin{bmatrix} \sqrt{R^2 - a^2} \\ 0 \\ a \end{bmatrix}, {}^{B}n_2 = 1/R \begin{bmatrix} (\sqrt{R^2 - b^2})\, C\psi_2 \\ (\sqrt{R^2 - b^2})\, S\psi_2 \\ b \end{bmatrix}, $$

$$ {}^{B}n_3 = 1/R \begin{bmatrix} (\sqrt{R^2 - c^2})\, C\psi_3 \\ (\sqrt{R^2 - c^2})\, S\psi_3 \\ c \end{bmatrix} $$

Remarks: In the three preceding cases, one of the object's dimensions is taken as unknown (ℓ for a parallelopiped, R for a cylinder and a sphere). The computed value can, thus, be compared with the measured dimension. This offers an additional way to validate the model since this dimension is well known. In Section 4, the obtained results show that this deviation is lower than a few tenth of millimeter.

4. Experimental Validation

We have pointed out, in Section 3, that six new unknowns were to be selected among the 12 articular parameters to obtain a nonlinear system of 24 equations to 24 unknowns. There are $C_{12}^6 = 920$ possibilities to choose these unknowns. Intuitively, one can easily imagine that it is better to take the values of the abduction-adduction movement articular parameters as unknowns, because that does not lock the configuration space of each finger in only one plan. All the choices were examined for several object motions. To check this assumption and to validate the model, first we use an experimental device that is able to lock five degrees of freedom of the object and keep free one translation or one rotation of the object. Thus, the computed trajectories are easily compared with the real trajectories. For instance, Fig. 11 shows a device that only allows the φ_3 rotation of the object around the z_b-axis, which is collinear with the z-axis of the palm frame **P**.

We observed that all the tests which take the joint parameters of abduction-adduction (q04 for the thumb, q11 and q12 for the fingers) as unknown of the problem (case 1) give similar results to those of Fig. 12a. The computed parameters q_{0j}^* and q_{1j}^* are compared with those measured by the exoskeleton (q_{0j}, q_{1j}) during the rotation of a cylinder. The deviations Δij between the recorded joint parameters (q_{ij}) and those computed (q_{ij}^*) are shown in Fig. 12b. Those deviations do not exceed 1.2°, which is sufficient for the application. We have to specify that during the manipulation with the exoskeleton, an undesired sliding of the object in the fingers can occur. Therefore, to eliminate the possible sliding, the model adjusts the object trajectory or modifies the joint parameters selected as unknowns. Thus, comparisons between real trajectories and computed trajectories can only be possible if the object does not slide.

When the abduction-adduction joint parameters are not taken as unknowns, the deviations Δij between the recorded parameters (q_{ij}) and computed parameters (q_{ij}^*) increase and for some cases the model does not converge. For example, Fig. 13 shows that there are significant deviations

https://doi.org/10.1017/S0263574707003736 Published online by Cambridge University Press

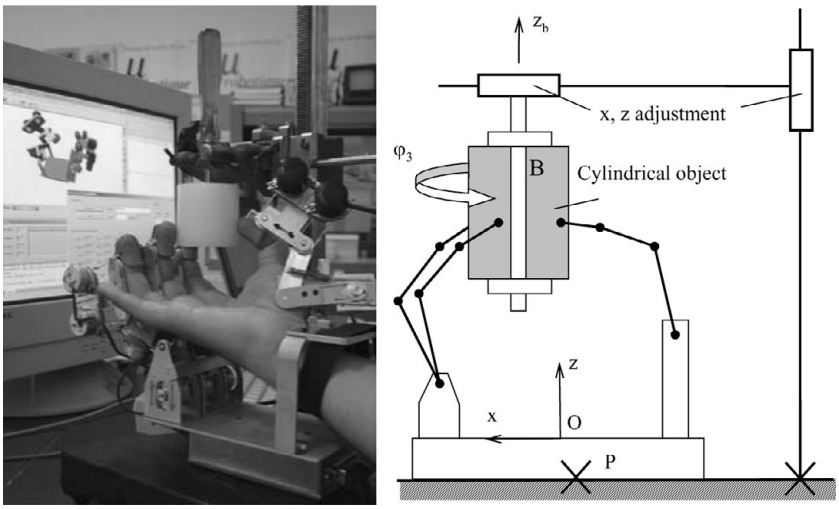

Fig. 11. Experimental device for a rotation around z.

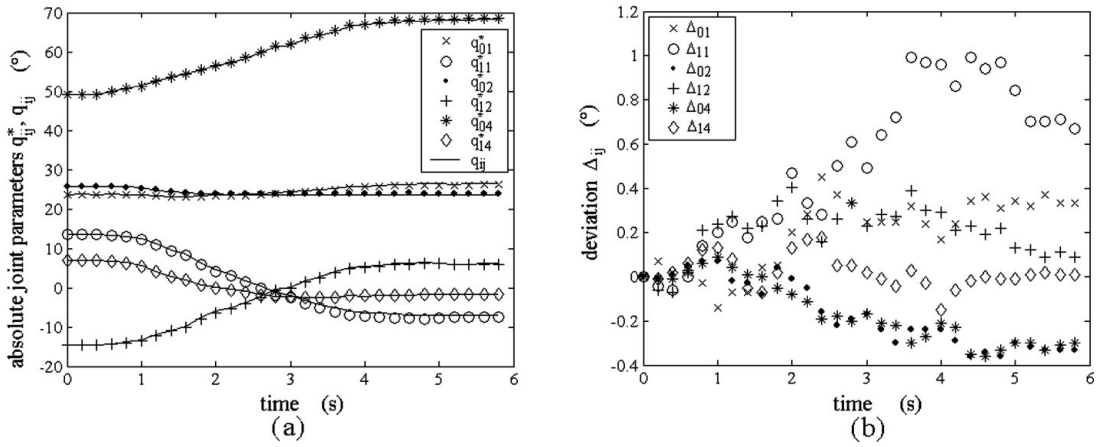

Fig. 12. (a) Computed parameters (q_{ij}^*) and measured parameters (q_{ij}) for q_0 and q_1 taken as unknowns for the rotation of a cylinder around the z-axis. (b) Deviations $\Delta_{ij} = q_{ij} - q_{ij}^*$.

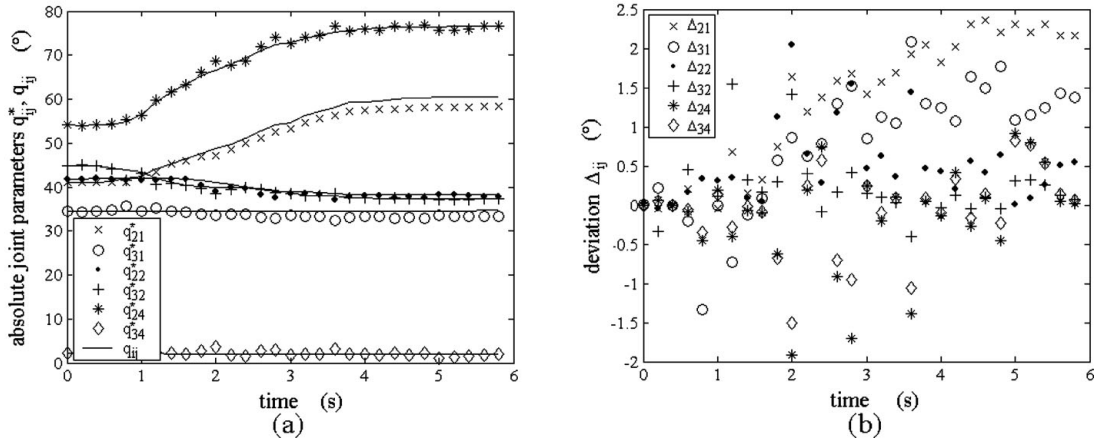

Fig. 13. (a) Computed parameters (q_{ij}^*) and measured parameters (q_{ij}) for q_2 and q_3 taken as unknowns for the rotation of a cylinder around z. (b) Deviations $\Delta_{ij} = q_{ij} - q_{ij}^*$.

when q_{2j} and q_{3j} are taken as unknowns of the problem (case 2).

For this trajectory (cylinder rotation), Figs. 14a and c shows the operational coordinates defining the object movement (case 1 and case 2). Figure 14b and d describes in plan the fingers' path on the object (case 1 and case 2). For this example, the cylinder described a rotation φ_3 approximately with a displacement of 63°. The computed diameter of the cylinder is equal to 51.6 mm whereas the real diameter is equal to 51.2 mm. This small deviation is very satisfactory,

https://doi.org/10.1017/S0263574707003736 Published online by Cambridge University Press

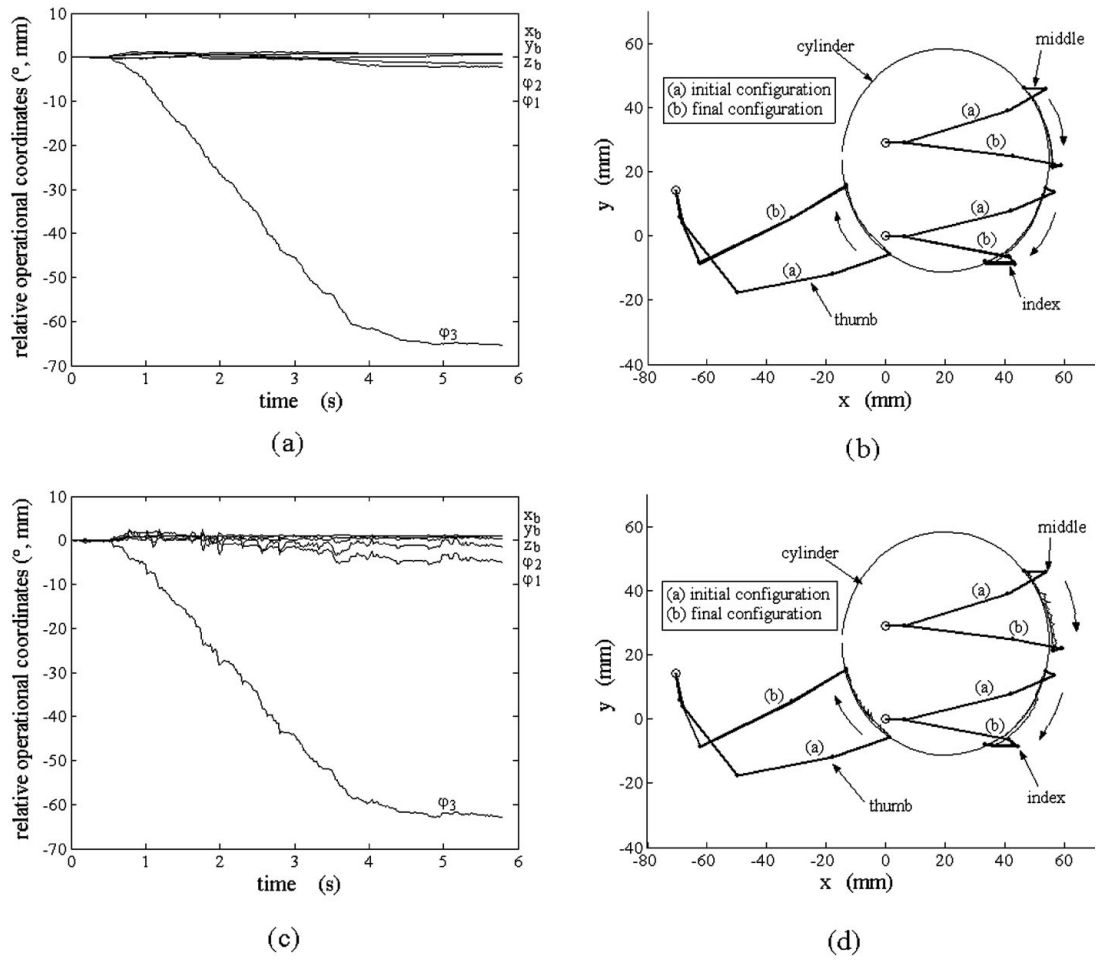

Fig. 14. (a), (c) Evolution of the operational coordinates. (b), (d) Fingers' path on the object.

all the more since it remains lower than a few tenths of a millimeter for the different sizes and forms of objects we have tested. Figure 14a and b shows that the computed trajectory corresponding to case 1 is close to the real trajectory of the object with a small deviation of the trajectory on the other operational coordinates. Figure 14c and d, corresponding to case 2, shows a more disturbed movement with trajectories that deviate from the real trajectories. Thus, these results consolidate the choice to take the parameters of abduction-adduction as unknowns.

We then reproduced this rotation with a free cylinder (without the device of Fig. 11). In this case, the goal of the operator is to choose an initial grasp in order to execute the largest rotation allowed. The results are shown in Figs. 15

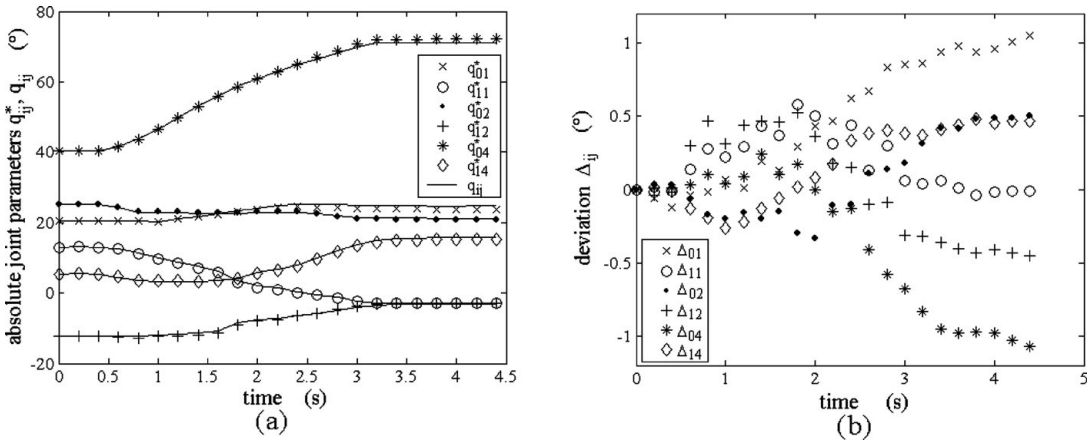

Fig. 15. (a) Calculated parameters (q^*_{ij}) and measured parameters (q_{ij}) for q_0 and q_1 taken as unknowns for a desired rotation of a cylinder around the z_b-axis. (b) Deviation $\Delta_{ij} = q_{ij} - q^*_{ij}$.

https://doi.org/10.1017/S0263574707003736 Published online by Cambridge University Press

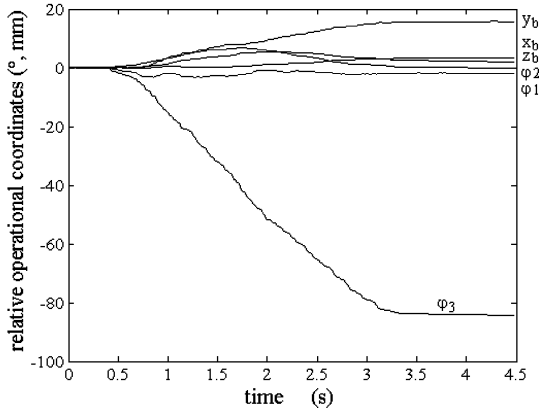

Fig. 16. Operational coordinates of the object.

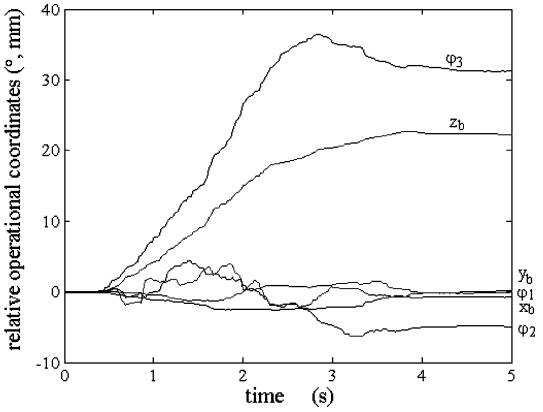

Fig. 18. Operational coordinates of the object.

and 16. In Fig. 15a and b, we can observe that the deviations between the calculated and the measured parameters have the same order of magnitude as previously. In Fig. 16, the corresponding rotation φ_3 has indeed a largest range approximately of 80°. However, an undesired translation along the y-axis approximately of 15 mm appears. The other motion parameters are negligible.

Finally, we present in Figs. 17 and 18 the results for a combined translation and rotation of a parallelopiped where dimensions are $20 \times 44, 8 \times 80\,\text{mm}^3$. The software computes a width of the object according to the grasp axis equal to 45.1 mm instead of 44.8 mm. The deviation between these two values remains satisfactory. For this combined motion, the deviations between the calculated parameters and the measured parameters for q_0 and q_1 (Figs. 17a and b), are still satisfactory. This proves the robustness of the model. We can verify in Fig. 18, that the object described a combined motion of 20 mm for the translation and of 35° for the rotation φ_3.

5. Conclusion

We presented an efficient approach that allows us to easily generate trajectories of objects handled by the LMS mechanical hand. This approach is based on learning and uses an exoskeleton that has kinematics and dimensions identical to the LMS mechanical hand. The exoskeleton and its exploitation were presented. Starting from a reliable model, which is proposed, the only knowledge of the articular parameters and the partial knowledge of initial grasp enable us to determine the trajectory of the object. The proposed approach has been checked by a CAD software as well as by the mechanical hand. The joint parameters given by the exoskeleton are directly loaded on the mechanical hand-control device which solves the grasp stability in real time during the manipulation of object. The behavior of the mechanical hand and the handled object in this way is very satisfactory. Since the exoskeleton has the same capability of movement as the mechanical hand, this feature is used to exploit the ability, the experiment, and the adaptability of a

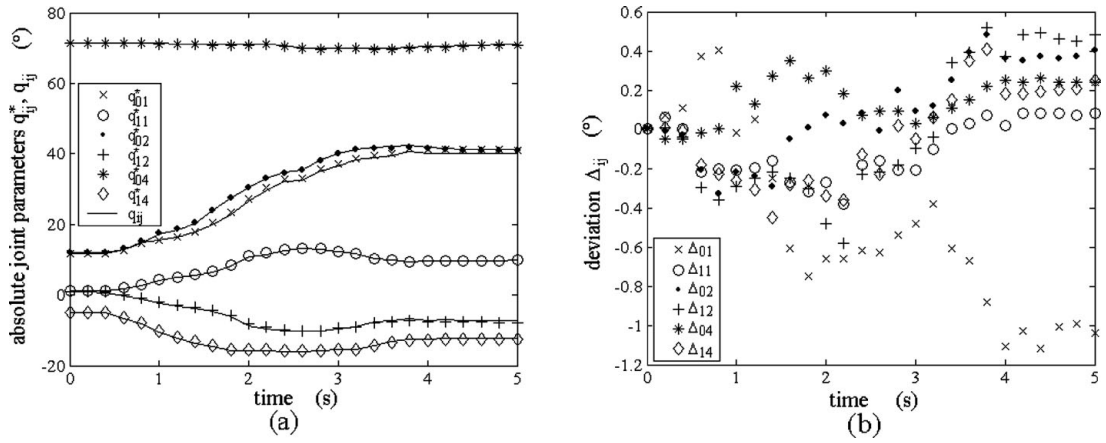

Fig. 17. (a) Calculated parameters (q^*_{ij}) and measured parameters (q_{ij}) for q_0 and q_1 taken as unknowns for a combined translation and rotation of a parallelopiped. (b) Deviation $\Delta_{ij} = q_{ij} - q^*_{ij}$.

https://doi.org/10.1017/S0263574707003736 Published online by Cambridge University Press

human operator for the manipulation of objects through the exoskeleton. The obtained results show that this approach is well adapted for trajectory planning.

References

1. M. Bouzit, G. Burdea, G. Popescu and R. Boian, "The Rutgers Master II—New design force-feedback glove," *IEEE/ASME Trans. Mechatronics* **7**(2), 256–263 (2002).
2. R. N. Rohling, J. M. Hollerbach and S. C. Jacobsen, "Optimized fingertip mapping: A general algorithm for robotic hand teleoperation" *Presence* **2**(3), 203–220 (1993).
3. M. Bouzit, P. Coiffet and G. Burdea, "The LRP Dextrous Hand Master," *Proceedings of the Virtual Reality Systems Fall'93*, New York (Sep., 1993).
4. B. H. Choi, H. R. Choi and W. J. Chung, "Two-fingered Hand Exoskeleton Driven by Ultrasonic Motor," *Proceedings of the 3rd IWAM* (Dec. 1999) pp. 389–394.
5. T. Koyama, I. Yamano, K. Takemura and T. Maeno, "Multi-Fingered Exoskeleton Haptic Device Using Passive Force Feedback for Dexterous Teleoperation," *Proceedings of the IEEE/RSJ International Conference on Intelligent Robots and Systems* (Oct. 2002) pp. 2905–2910.
6. T. Mouri, H. Kawasaki and K. Umebayashi, "Developments of New Anthropomorphic Robot Hand and its Master Slave System," *Proceedings of the 2005 IEEE/RSJ International Conference on Intelligent Robots and Systems* (2005) pp. 3474–3479.
7. 5DT Data Glove Series [Online]. Available: http://www.vrlogic.com (2007).
8. CyberGlove® II Wireless Data Glove [Online]. Available: http://www.immersion.com/3d/phprint.php (2007).
9. Wireless Motion Capture Glove [Online]. Available: http://motionanalysis.com/about_mac/talon.html (2007).
10. M. Fischer, P. van der Smagt and G. Hirzinger, "Learning Techniques in a Dataglove Based Telemanipulation System for the DLR Hand," *Proceedings of the IEEE International Conference on Robotics & Automation* (1998) pp. 1603–1608.
11. H. Hu, X. Gao, J. Li, J. Wang and H. Liu, "Calibrating Human Hand for Teleoperating the HIT/DLR Hand," *Proceedings of the IEEE International Conference on Robotics and Automation* (Apr. 2004) pp. 4571–4576.
12. W. B. Griffin, R. P. Findley, M. L. Turner and M. R. Cutkosky, "Calibration and Mapping of a Human Hand for Dexterous Telemanipulation," *Proceeding of the ASME IMECE Symposium on Haptic Interfaces for Virtual Environments and Teleoperator Systems* (2000), vol. 69, no. 2 pp. 1145–1152.
13. F. Kahlesz, G. Zachmann and R. Klein, "Visual-fidelity dataglove calibration," *Proceedings of the Computer Graphics International* (June 2004) pp. 403–410.
14. S. Zeghloul, B. Blanchard and M. Ayrault, "SMAR: A robot modeling and simulation system," *Robotica* **15** (P. 1), pp. 63–73 (1997).
15. J. P. Gazeau, S. Zeghloul, M. Arsicault and J. P. Lallemand, "The LMS Hand: Force and Position Controls in the Aim of the Fine Manipulation of Objects," *Proceedings of the IEEE International Conference on Robotics and Automation*, Seoul, Korea (May 2001) pp. 2642–2648.
16. J. P. Gazeau, S. Zeghloul, M. Arsicault and J. P. Lallemand, "Manipulation with the LMS mechanical hand: a strategy for fingertip manipulation tasks," *J. Eur. Autom.* **36**(9), 1205–1219 (2002).
17. J. P. Gazeau, S. Zeghloul and G. Ramirez, "Manipulation with a polyarticulated mechanical hand: a new efficient real-time method for computing fingertip forces for a global manipulation strategy," *Robotica* **23**, 479–490 (2005).
18. J. Kerr and B. Roth, "Analysis of multifingered hands" *Int. J. Robot. Res.* **4**(4), 3–17 (1986).

Appendix

We consider hemispherical fingertips with a known radius **r**. The manipulated objects are convex. Thus, in frame **T**, the position of the contact point **C** and its normal are defined by

$$ {}^{\mathrm{T}}C = \begin{bmatrix} rC\alpha C\beta \\ rC\alpha S\beta \\ rS\alpha \end{bmatrix} \quad \text{and } {}^{\mathrm{T}}n = \begin{bmatrix} C\alpha C\beta \\ C\alpha S\beta \\ S\alpha \end{bmatrix} $$

Likewise, in frame **B**, the same position of the contact point **C** and its normal are defined by

$$ {}^{\mathrm{B}}C = \begin{bmatrix} x(\eta,\ \zeta) \\ y(\eta,\ \zeta) \\ z(\eta,\ \zeta) \end{bmatrix} \quad \text{and } {}^{B}n = \begin{bmatrix} x_n(\eta,\ \zeta) \\ y_n(\eta,\ \zeta) \\ z_n(\eta,\ \zeta) \end{bmatrix} $$

where x, y, z, x_n, y_n, and z_n depend on the geometry of the manipulated object.

Moreover, we introduce the following notations:

${}^{P}O_{\mathrm{T}} = [x_t,\ y_t,\ z_t]^{\mathrm{T}}$ is the matrix of components of vector $\mathrm{OO_T}$ with respect to the **P** frame.

${}^{P}O_{B} = [x_b, y_b, z_b]^{\mathrm{T}}$ is the matrix of components of vector $\mathrm{OO_B}$ with respect to the **P** frame.

- Thus, Eq. (1) can be expressed as.

$$ {}^{P}O_{\mathrm{T}} + {}^{P}A_{\mathrm{T}} \cdot {}^{\mathrm{T}}C = {}^{P}O_{B} + {}^{P}A_{B} \cdot {}^{B}C \qquad \text{(A1)} $$

or

$$ \begin{bmatrix} x_t \\ y_t \\ z_t \end{bmatrix} + {}^{P}A_{\mathrm{T}} \begin{bmatrix} rC\alpha C\beta \\ rC\alpha S\beta \\ rS\alpha \end{bmatrix} = \begin{bmatrix} x_b \\ y_b \\ z_b \end{bmatrix} + {}^{P}A_{B} \begin{bmatrix} x \\ y \\ z \end{bmatrix} $$

where ${}^{P}A_{\mathrm{T}}$ is the transform matrix between reference frames **P** and **T**.

The matrix ${}^{P}A_{\mathrm{T}}$ is given by:

For finger:

$$ {}^{P}A_{\mathrm{T}} = \begin{bmatrix} C_0C_1C_{23} - S_0S_{23} & -S_0S_1 & C_0C_1S_{23} + S_0C_{23} \\ S_1C_{23} & C_1 & S_1S_{23} \\ -S_0C_1C_{23} - C_0S_{23} & S_0S_1 & -S_0C_1S_{23} + C_0C_{23} \end{bmatrix} $$

For the thumb: $ {}^{P}A_{\mathrm{T}} = \begin{bmatrix} C_{123} & -S_{123} & 0 \\ C_0S_{123} & C_0C_{123} & -S_0 \\ S_0S_{123} & S_0C_{123} & C_0 \end{bmatrix}. $

The fingers' bases are oriented of an angle γ around z with respect to the palm. So, to be expressed in the reference frame **P**, ${}^{P}A_{\mathrm{T}}$ is multiplied by the following transform matrix A_γ:

$$ A_\gamma = \begin{bmatrix} C_\gamma & -S_\gamma & 0 \\ S_\gamma & C_\gamma & 0 \\ 0 & 0 & 1 \end{bmatrix}. $$

https://doi.org/10.1017/S0263574707003736 Published online by Cambridge University Press

${}^{P}A_{B}$ is the transform matrix between **P** and **B** using pitch, yaw, and roll angles φ_1, φ_2, and φ_3, i.e.

$$
{}^{P}A_{B} = \begin{bmatrix} C\varphi_2 C\varphi_3 & -C\varphi_2 S\varphi_3 & S\varphi_2 \\ C\varphi_1 S\varphi_3 + S\varphi_1 S\varphi_2 C\varphi_3 & C\varphi_1 C\varphi_3 - S\varphi_1 S\varphi_2 S\varphi_3 & -S\varphi_1 C\varphi_2 \\ S\varphi_1 S\varphi_3 - C\varphi_1 S\varphi_2 C\varphi_3 & S\varphi_1 C\varphi_3 + C\varphi_1 S\varphi_2 S\varphi_3 & C\varphi_1 C\varphi_2 \end{bmatrix}.
$$

- Relation (2) becomes

$$
{}^{P}A_{\mathrm{T}} \cdot {}^{\mathrm{T}}n = {}^{P}A_{B} \cdot {}^{B}n \tag{A2}
$$

or

$$
{}^{P}A_{\mathrm{T}} \begin{bmatrix} C_\alpha C_\beta \\ C_\alpha S_\beta \\ S_\alpha \end{bmatrix} = {}^{P}A_{B} \begin{bmatrix} x_n \\ y_n \\ z_n \end{bmatrix}.
$$

- In differential form, relation (3) can be written

$$
\dot{O}_{\mathrm{T}} + \omega_{\mathrm{T}} \wedge \left({}^{P}A_{\mathrm{T}} \cdot {}^{\mathrm{T}}C\right) = \dot{O}_{B} + \Omega_{B} \wedge \left({}^{P}A_{B} \cdot {}^{B}C\right)
$$

where the dot denotes the time derivative. Thus, the small displacements model is given by

$$
\boldsymbol{\delta}\mathrm{O}_{\mathrm{T}} + \boldsymbol{\delta\omega}_{\mathrm{T}} \wedge {}^{\mathrm{T}}\mathbf{C}^{i-1} = \boldsymbol{\delta}\mathrm{O}_{\mathrm{B}} + \boldsymbol{\delta\Omega}_{\mathrm{B}} \wedge {}^{\mathrm{B}}\mathbf{C}^{i-1}
$$

where $\boldsymbol{\delta}\mathrm{O}_{\mathrm{T}}$ and $\boldsymbol{\delta}\mathrm{O}_{B}$ are translation vectors of points O_{T} and O_B between iteration i and iteration $i-1$.

$\boldsymbol{\delta\omega}_{\mathrm{T}}$ and $\boldsymbol{\delta\Omega}_{\mathrm{B}}$ are angular velocity vectors relatively to the distal phalanx and the object between iteration i and iteration $i-1$.

${}^{\mathrm{T}}\mathbf{C}^{i-1}$ and ${}^{B}C^{i-1}$ are position vectors of point **C**, respectively, to frame **T** and frame **B** at iteration $i-1$.

We define ${}^{P}J_{\omega}$ the rotational Jacobian matrix of the fingertip in frame **P** as

$$
\boldsymbol{\delta\omega}_{\mathrm{T}} = {}^{P}J_{\omega}\left(q_0^{i-1},\ q_1^{i-1},\ q_2^{i-1},\ q_3^{i-1}\right) \cdot \boldsymbol{\delta}\mathbf{q}
$$

where

$$
\boldsymbol{\delta}\mathbf{q} = [\delta q_0,\ \delta q_1,\ \delta q_2,\ \delta q_3]^{\mathrm{T}},
$$

${}^{P}J_{\omega} = A_\gamma J_\omega (A_\gamma$ previously described),

$$
J_\omega = \begin{bmatrix} 0 & -S_0 & C_0S_1 & C_0S_1 \\ 0 & C_0 & S_0S_1 & S_0S_1 \\ 1 & 0 & C_1 & C_1 \end{bmatrix} \quad \text{for a finger,}
$$

$$
J_\omega = \begin{bmatrix} 0 & S_0 & S_0 & S_0 \\ 0 & -C_0 & -C_0 & -C_0 \\ 1 & 0 & 0 & 0 \end{bmatrix} \quad \text{for the thumb.}
$$

The global motion of the object can be defined by the vector components $\delta\Omega_B = [\delta\theta_x,\ \delta\theta_y,\ \delta\theta_z]^{\mathrm{T}}$ in frame B.

With these notations, Eq. (3) can be expressed as

$$
\begin{aligned} &\delta O_{\mathrm{T}} + \left({}^{P}J_{\omega}\left(q_0^{i-1}, q_1^{i-1}, q_2^{i-1}, q_3^{i-1}\right) \cdot \delta q_i\right) \\ &\times \wedge \left({}^{P}A_{\mathrm{T}}^{i-1} \cdot {}^{\mathrm{T}}C^{i-1}\right) \\ &= \delta O_B + \left({}^{P}A_{B}^{i-1} \cdot \delta\theta\right) \wedge \left({}^{P}A_{B}^{i-1} \cdot {}^{B}C^{i-1}\right) \end{aligned} \tag{A3}
$$

where ${}^{P}A_{\mathrm{T}}^{i-1}$ is the transform matrix between **P** and **T** at iteration $i-1$ and ${}^{P}A_{B}^{i-1}$ is the transform matrix between **P** and **B** at iteration $i-1$.

We can note that the last equation contains the six unknowns concerning the position and orientation of the object, i.e., δO_B and $\delta\theta$.

https://doi.org/10.1017/S0263574707003736 Published online by Cambridge University Press